IL-13Rα2 and IL-10 coordinately suppress airway inflammation, airway-hyperreactivity, and fibrosis in mice

Mark S. Wilson,[1] Eldad Elnekave,[1] Margaret M. Mentink-Kane,[1] Marcus G. Hodges,[2] John T. Pesce,[1] Thirumalai R. Ramalingam,[1] Robert W. Thompson,[1] Masahito Kamanaka,[3] Richard A. Flavell,[3] Andrea Keane-Myers,[2] Allen W. Cheever,[4] and Thomas A. Wynn[1]

[1]Immunopathogenesis Section, Laboratory of Parasitic Diseases, and
[2]Laboratory of Allergic Diseases, National Institute of Allergy and Infectious Diseases (NIAID), NIH, Bethesda, Maryland, USA.
[3]Section of Immunobiology, Yale University School of Medicine, New Haven, Connecticut, USA. [4]Biomedical Research Institute, Rockville, Maryland, USA.

Development of persistent Th2 responses in asthma and chronic helminth infections are a major health concern. IL-10 has been identified as a critical regulator of Th2 immunity, but mechanisms for controlling Th2 effector function remain unclear. IL-10 also has paradoxical effects on Th2-associated pathology, with IL-10 deficiency resulting in increased Th2-driven inflammation but also reduced airway hyperreactivity (AHR), mucus hypersecretion, and fibrosis. We demonstrate that increased IL-13 receptor α 2 (IL-13Rα2) expression is responsible for the reduced AHR, mucus production, and fibrosis in BALB/c IL-10$^{-/-}$ mice. Using models of allergic asthma and chronic helminth infection, we demonstrate that IL-10 and IL-13Rα2 coordinately suppress Th2-mediated inflammation and pathology, respectively. Although IL-10 was identified as the dominant antiinflammatory mediator, studies with double IL-10/IL-13Rα2–deficient mice illustrate an indispensable role for IL-13Rα2 in the suppression of AHR, mucus production, and fibrosis. Thus, IL-10 and IL-13Rα2 are both required to control chronic Th2-driven pathological responses.

Introduction

Th2 responses induced by allergen exposure (1) or chronic helminth infection (2) can cause significant tissue damage, remodeling, and fibrosis. Although the Th2 response is characterized by many cytokines, including IL-4, IL-5, IL-9, IL-10, IL-13, IL-21, and IL-17E (IL-25), IL-13 is of particular interest because it appears to be a key effector cytokine (3, 4). Animal models have highlighted the pivotal role of IL-13 in mediating many of the features of asthma. For example, delivering IL-13 directly to the airways of mice (5–7) or overexpressing IL-13 in the lungs (7) triggers Th2-polarized inflammation with increased chemokine response (8), adhesion molecule expression (9), mucus hypersecretion, and airway hyperreactivity (AHR) (10, 11), all features of asthma. The critical role of IL-13 was confirmed in IL-13–blocking studies (5, 6). Chronic bouts of Th2-associated inflammation in idiopathic pulmonary fibrosis (12), ulcerative colitis (13), or helminth infection (14, 15) are also associated with IL-13–mediated pathologies. Given that IL-13 is the foremost Th2 cytokine mediating Th2-dependent disease, it is important to understand how IL-13 effector function is regulated in distinct tissues and in acute and chronic Th2-driven disorders.

IL-13 effector function can be regulated by a decoy receptor, IL-13 receptor α 2 (IL-13Rα2) (16), adding an additional level of control to Th2 responses. IL-13Rα2, unlike the type 2 IL-4 receptor (IL-4Rα/IL-13Rα1), does not activate Stat6 signaling, but instead proportionally reduces IL-13 (17, 18) and in some cases IL-4 activity (19). Although the function of IL-13 in allergic diseases has been studied extensively, IL-13Rα2 has received much less attention (20, 21). IL-13Rα2 was recently shown to control bronchial reactivity following IL-13 stimulation in vitro (21). Nevertheless, the role of the endogenous IL-13Rα2 has not to our knowledge been previously investigated in the lung.

It is well known that IL-10 can regulate T cell proliferation (22) and cytokine secretion (23). However, it remains controversial whether IL-10 suppresses or promotes Th2 responses (24–32). Administration of rIL-10 (33, 34) or IL-10–expressing CD4$^+$CD25$^+$ Tregs (35, 36) to allergen-sensitized mice suppresses Th2 cytokine secretion, while related studies reported increased AHR following exposure to IL-10 (33), suggesting that Th2 development and Th2-driven pathologies are differentially regulated by IL-10. This hypothesis is supported by studies with IL-10$^{-/-}$ mice; however, in these experiments Th2 cytokine production increased, while development of AHR either decreased following allergen challenge (37, 38) or remained unchanged despite increased inflammation (39).

Because IL-10 and IL-13Rα2 are both capable of modulating IL-13 effector function, we examined whether the regulatory activities of IL-10 were associated with changes in IL-13Rα2 production and/or function. We found that IL-10 applies an essential brake on inflammation, with IL-10$^{-/-}$ mice presenting increased inflammatory responses but, paradoxically, decreased AHR following airway allergen challenge and reduced liver fibrosis following acute *Schistosoma mansoni* infection. The reduced pathological responses in IL-10$^{-/-}$ mice were associated with increased IL-13Rα2 production. Therefore, to determine whether the observed changes in IL-13Rα2 expression were responsible for the modified pathological responses in IL-10$^{-/-}$ mice, we generated IL-10$^{-/-}$IL-13Rα2$^{-/-}$ double-KO (dKO) mice. Strikingly, we found that dKO mice developed significantly more immunopathology and inflammation compared with either single-KO mouse, demonstrating that IL-13Rα2 cooperates with IL-10 to control Th2-driven pathologies.

Nonstandard abbreviations used: AHR, airway hyperreactivity; BAL, bronchoalveolar lavage; COL III, collagen III; dKO, double-KO; IL-13Rα2, IL-13 receptor α 2; Penh, enhanced pause; R_L, lung resistance; SEA, soluble egg antigen.

Conflict of interest: The authors have declared that no conflict of interest exists.

Citation for this article: *J. Clin. Invest.* **117**:2941–2951 (2007). doi:10.1172/JCI31546.

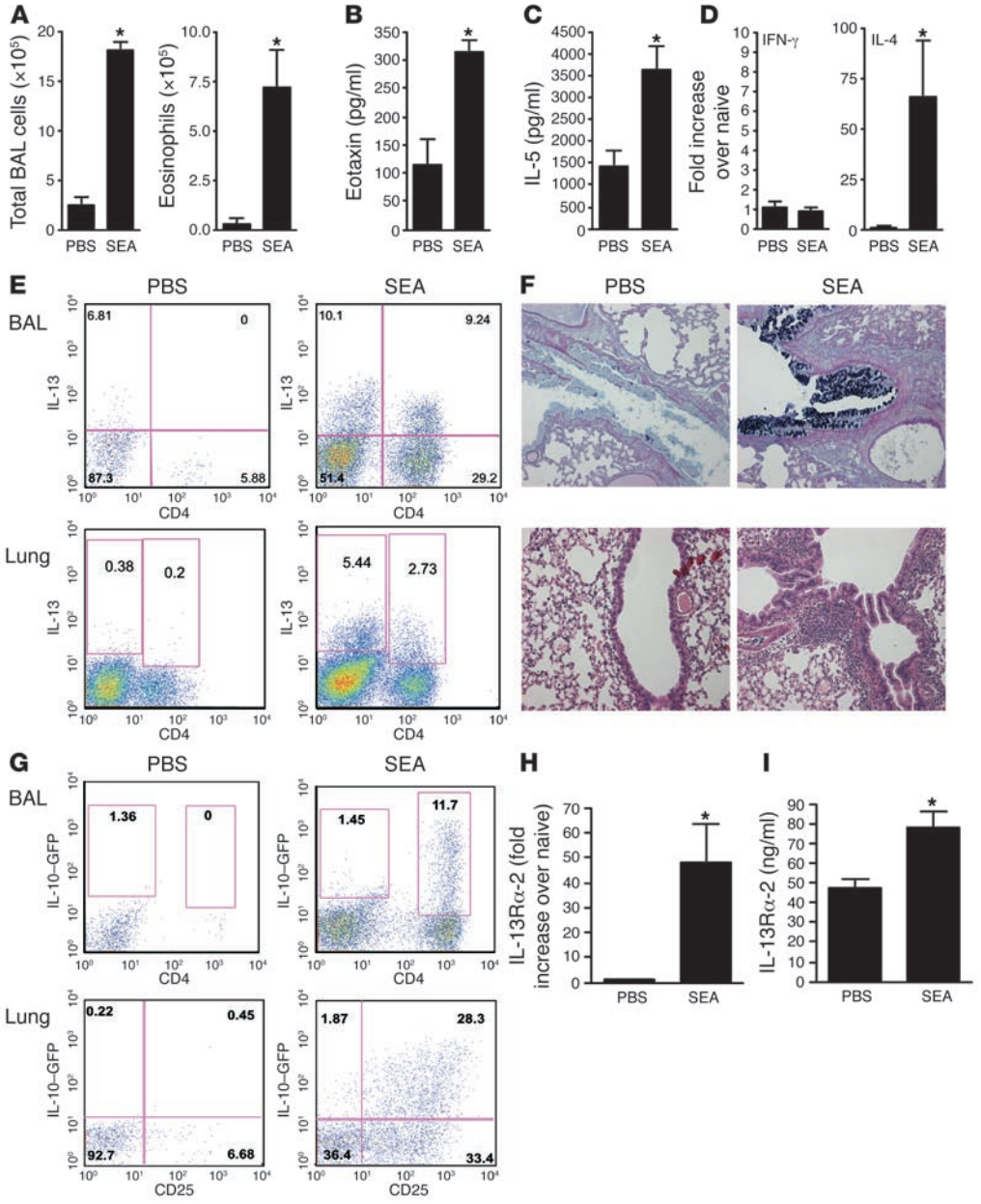

Figure 1

Th2-polarized SEA-induced airway inflammation. Animals were sensitized with 10 μg SEA on days 1 and 14, followed by 2 intratracheal airway challenges with 10 μg SEA on days 28 and 31. Animals were euthanized 24 hours after the final airway challenge. *$P < 0.05$, Mann-Whitney *U* test. (**A**) Total airway infiltrates and airway eosinophilia recovered in BAL. (**B**) BAL fluid eotaxin levels measured by ELISA. (**C**) BAL fluid IL-5 levels measured by ELISA. (**D**) Lung tissue mRNA, *IFNγ* (Th1) and *IL-4* (Th2). (**E**) BAL and lung cells stimulated with PMA and ionomycin with brefeldin A for 3 hours and then stained with anti-CD4 (APC) and anti-IL-13 (PE) before acquisition and analysis by FACS. (**F**) Five-micrometer sections were cut from paraffin-embedded lung tissue and stained with H&E (lower panels) to show cellular infiltration or alcian blue–PAS (upper panels) showing mucin$^+$ goblet cells lining the airways. The mucin response to SEA was 7+, while the inflammatory response to PBS was 2+ and to SEA, 4+. Five lungs from each group were scored in a blinded fashion; original magnification, ×100. (**G**) Lung cells and BAL recoveries from C57BL/6 IL-10–GFP mice were stained with anti-CD4 (APC) and anti-CD25 (PE) for lung cells, with GFP expression observed in the FL1 channel. (**H**) RNA was extracted from lung tissue, with IL-13Rα2 mRNA quantified by quantitative reverse transcription PCR (qRT-PCR). (**I**) Soluble IL-13Rα2 was measured by ELISA, in serum collected from mice bled 24 hours after the last airway challenge.

Results

Acute Th2-driven airway inflammation is controlled by IL-10 but not by IL-13Rα2. Intratracheal administration of a model allergen, soluble egg antigen (SEA), in SEA-sensitized mice provided a robust and reliable model of acute Th2-mediated allergic airway inflammation (Figure 1, A–F, and Supplemental Figure 1A; supplemental material available online with this article; doi:10.1172/JCI31546DS1), characterized by airway and tissue eosinophilia (Figure 1, A and F), bronchoalveolar

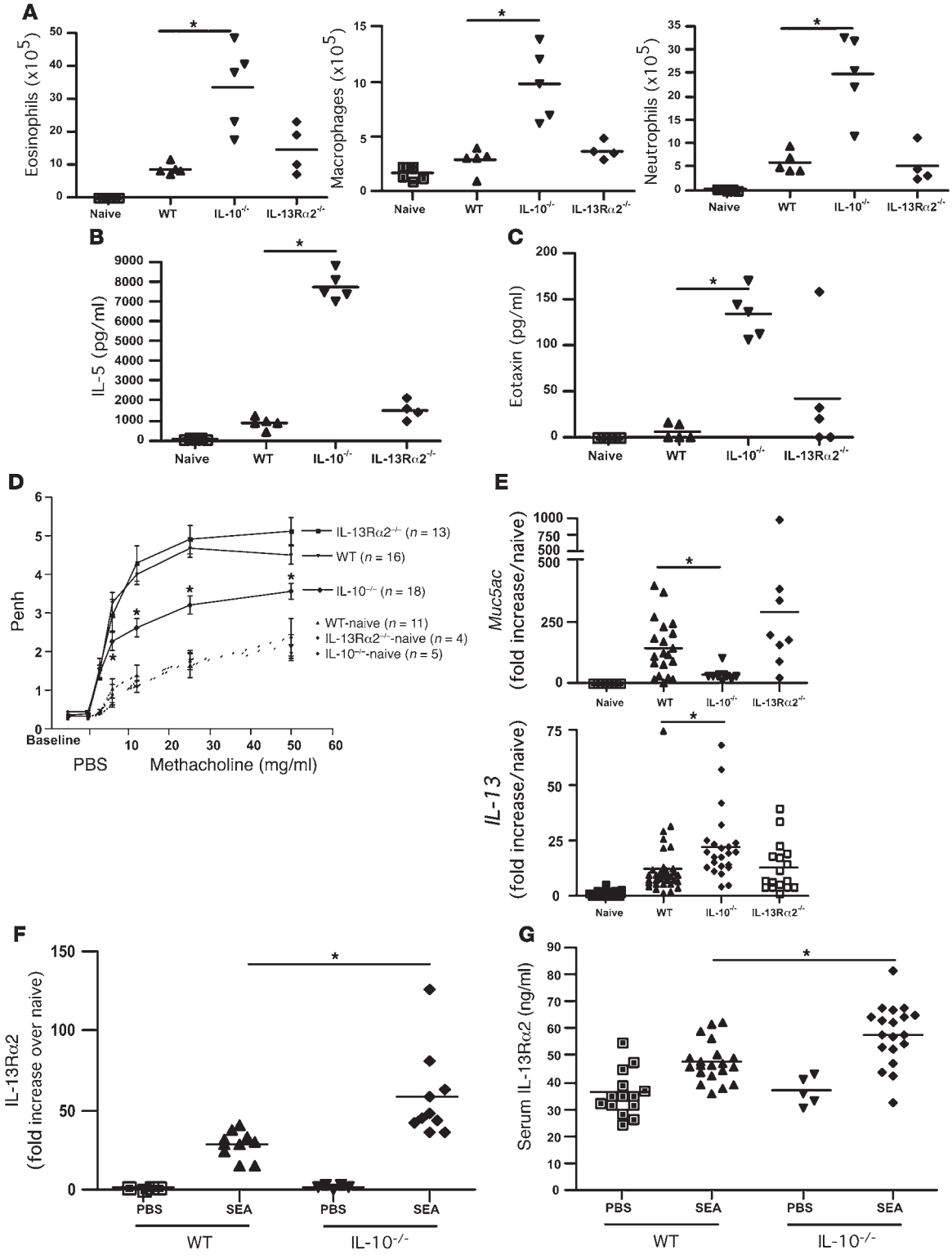

Figure 2

Airway inflammation, but not AHR, is regulated by IL-10. Animals were sensitized and challenged as in Figure 1. Animals were euthanized 24 hours after the final airway challenge. *$P < 0.05$, Mann-Whitney *U* test. (**A**) Airway eosinophils (left), neutrophils (right), and macrophages (center) recovered from BAL. (**B**) BAL fluid IL-5 levels measured by ELISA. (**C**) BAL fluid eotaxin levels measured by ELISA. (**D**) AHR. Penh measurements 24 hours after the final airway challenge using a Buxco system with mice exposed to increasing doses of methacholine. *n*, number of mice in each group. (**E**) RNA was extracted from lung tissue with *Muc5ac* (top) and *IL-13* (bottom) mRNA quantified by qRT-PCR. (**F**) RNA was extracted from lung tissue, with IL-13Rα2 mRNA quantified by qRT-PCR. (**G**) Soluble IL-13Rα2 was measured by ELISA in serum collected from mice bled 24 hours after the last airway challenge.

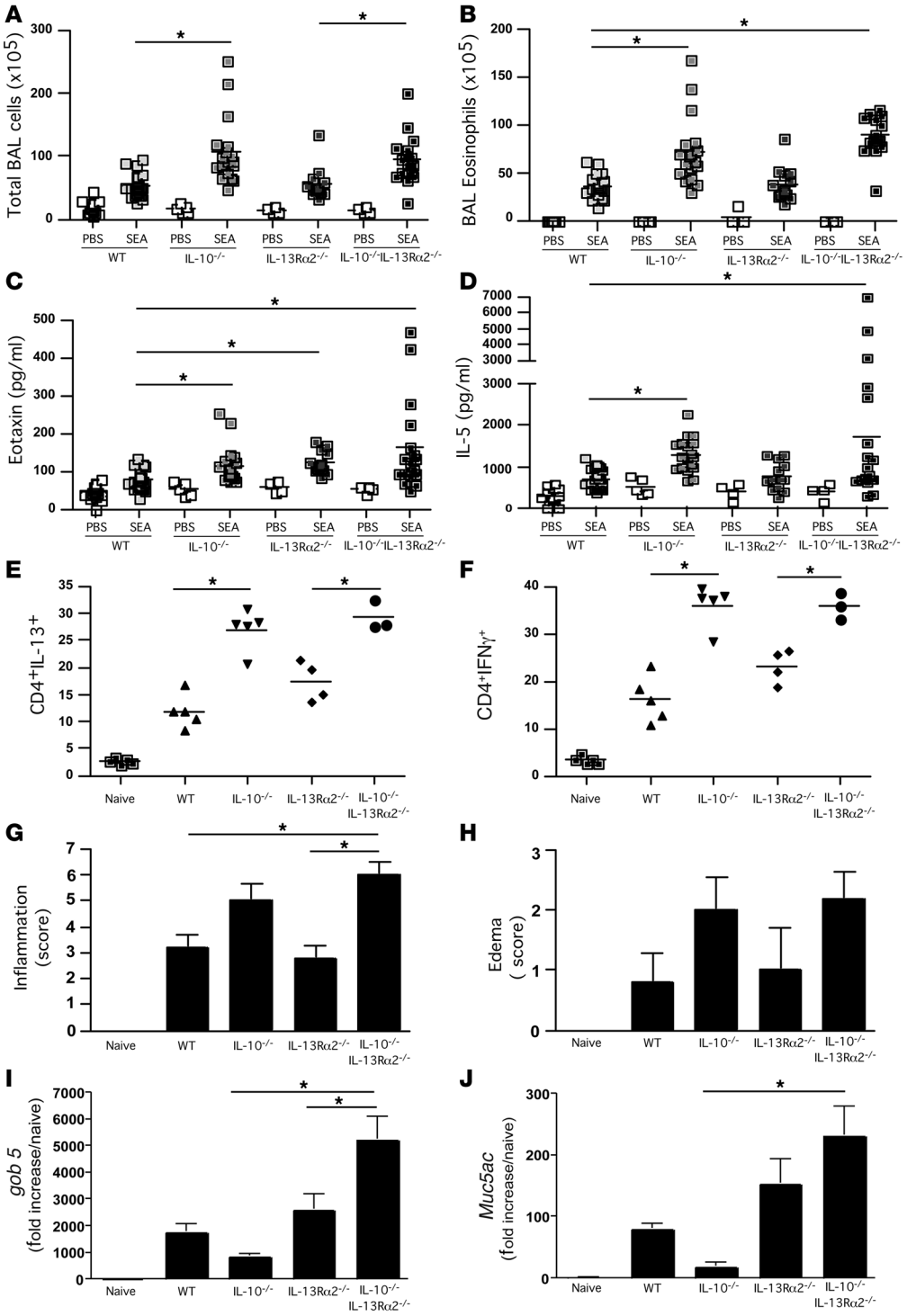

Figure 3
Exacerbated airway inflammation and airway pathology in IL-10$^{-/-}$IL-13Rα2$^{-/-}$ dKO mice following SEA challenge. Animals were sensitized and challenged as in Figure 1. Animals were euthanized 24 hours after the final airway challenge. *P < 0.05, 1-way ANOVA, except in Figure 3G, where a Kruskal-Wallis test was used. (**A**) Total airway infiltrates recovered in BAL. (**B**) Eosinophils recovered in BAL. (**C**) Eotaxin levels measured in BAL fluid by ELISA. (**D**) IL-5 levels measured by in BAL fluid by ELISA. (**E**) Lungs were excised, broken down into a single-cell suspension, and stimulated with PMA and ionomycin, with brefeldin A, for 3 hours and then stained with anti-CD4 (APC) and anti–IL-13 (PE) before cells were acquired and analyzed by FACS. (**F**) The procedure in **F** was identical to **E** apart from the final staining step using anti–IFN-γ and not anti–IL-13. (**G**) Perivascular/bronchial inflammation. H&E-stained sections from fixed and sectioned lungs were scored in a blinded fashion for cellular tissue infiltration. (**H**) Perivascular/bronchial edema. H&E-stained sections were scored in a blinded fashion for signs of edema. (**I**) RNA was extracted from lung tissue, with *gob 5* mRNA quantified by qRT-PCR. (**J**) As in **I**, except *Muc5ac* mRNA was quantified.

lavage (BAL) eotaxin (Figure 1B), and IL-5 (Figure 1C) secretion as well as elevated serum IL-5 and IgE levels (Supplemental Figure 1, B and C). There was also a significant increase in IL-4 but not IFN-γ mRNA in the lung (Figure 1D). In addition, cells capable of secreting high levels of IL-13 were recruited to the BAL and lung (Figure 1E), and there was a significant increase in goblet cells lining the airways (Figure 1F and Supplemental Figure 1D). Using IL-10–GFP reporter mice (40), we detected a significant expansion of IL-10^{+}CD4^{+}CD25^{+} T cells in the lung and a large increase in IL-10^{+}CD4^{+} T cells in the BAL (Figure 1G) following airway challenge. SEA also triggered a significant IL-13Rα2 response in the lung (Figure 1H) and serum (Figure 1I). Given that IL-10 and IL-13Rα2 were both markedly increased in the lung following SEA challenge, we investigated whether these proteins were regulating airway inflammation and/or lung function. Although germline deletion of IL-13Rα2 had no impact on cell recruitment (Figure 2A and Supplemental Figure 2A), IL-10 deficiency led to a 3-fold

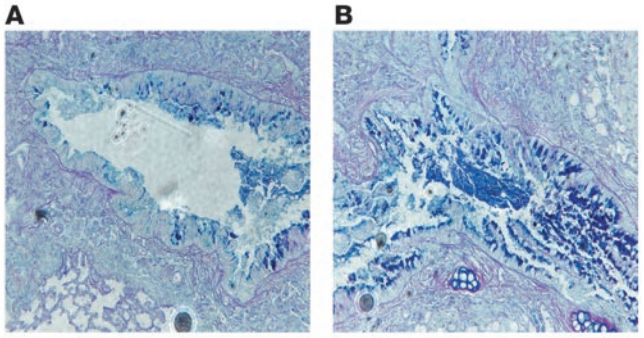

Figure 4
Removing IL-13Rα2 in IL-10$^{-/-}$ mice reveals a role for IL-13Rα2 in controlling goblet cell hyperplasia and mucus production. Animals were sensitized and challenged as in Figure 1. Animals were euthanized 24 hours after the final airway challenge. Alcian blue–PAS staining of fixed lung sections taken from IL-10$^{-/-}$ (**A**) and IL-10$^{-/-}$IL-13Rα2$^{-/-}$ dKO (**B**) mice; original magnification, ×100. Mucin-containing cells were graded as 2+ in **A** and 4+ in **B**. The inflammatory response was 8+ in both photomicrographs.

increase in total cells recruited to the airways (Supplemental Figure 2A), elevated numbers of eosinophils (Figure 2A), IL-5 (Figure 2B), and eotaxin (Figure 2C), as well as a significant increase in airway neutrophils and macrophages (Figure 2A).

AHR and mucus production are reduced in the absence of IL-10. AHR was also quantified in response to increasing doses of methacholine and expressed as enhanced pause (Penh). While SEA-challenged WT mice exhibited a significant increase in AHR, there was no significant difference noted in the IL-13Rα2$^{-/-}$ mice (Figure 2D). However, the IL-13Rα2$^{-/-}$ mice developed significantly stronger IL-10 responses (Supplemental Figure 2B), suggesting that there was some degree of immunological compensation in the absence of IL-13Rα2. Paradoxically, as reported previously in related studies investigating the function of IL-10 (38), AHR was significantly reduced in the IL-10$^{-/-}$ mice (Figure 2D) even though they had developed a markedly exacerbated inflammatory response (Figure 2A). *Muc5ac* (Figure 2E) and *gob 5* (Supplemental Figure 2C) mRNA expression was also reduced in the IL-10$^{-/-}$ mice. The observed pathological changes (reduced AHR and mucus) were difficult to explain, because in addition to displaying a robust inflammatory response, the IL-10$^{-/-}$ mice also developed significantly stronger IL-13 responses in the lung (Figure 2E).

IL-13Rα2 suppresses AHR and mucus production in IL-10$^{-/-}$ mice. The discrepant findings in IL-10$^{-/-}$ mice — increased inflammation and IL-13 production associated with reduced goblet cell hyperplasia, mucus production, and AHR — could be explained by changes in local and/or systemic IL-13Rα2 production. Indeed, we observed a significant increase in IL-13Rα2 mRNA in the lungs of SEA-challenged IL-10$^{-/-}$ mice when compared with WT animals (Figure 2F). There was also a significant increase in soluble IL-13Rα2 in the sera of IL-10$^{-/-}$ mice (Figure 2G). Therefore, to investigate whether the IL-13Rα2 response was regulating the development of AHR and mucus in the IL-10$^{-/-}$ mice, we generated animals that were simultaneously deficient in IL-13Rα2 and IL-10 (dKO mice). In contrast to the IL-13Rα2$^{-/-}$ mice, the dKO mice displayed an increased inflammatory response (Figure 3A) with elevated eosinophilia (Figure 3B), BAL eotaxin (Figure 3C), and IL-5 (Figure 3D), similar to IL-10$^{-/-}$ mice. In addition, intracellular cytokine staining of lung-associated lymphocytes indicated that there were significantly more CD4$^+$ T cells in the IL-10$^{-/-}$ and dKO lungs that were capable of producing IL-13 and IFN-γ when stimulated ex vivo (Figure 3, E and F). Histological scoring of lung sections confirmed that there was an increase in both inflammation (Figure 3G) and edema (Figure 3H) in the IL-10$^{-/-}$ and dKO mice. Nevertheless, despite developing similarly increased inflammatory responses, the IL-10$^{-/-}$ and dKO mice displayed completely divergent *gob 5* and *Muc5ac* mRNA responses (Figure 3, I and J). Indeed, the reduction in *gob 5* and *Muc5ac* mRNA observed in the IL-10$^{-/-}$ mice was reversed and even exacerbated in the dKO mice, suggesting that IL-13Rα2 was potently inhibiting the mucus response. Extensive mucus staining in the dKO airways confirmed the quantitative RT-PCR results (Figure 4).

We also examined whether airway function was altered in the dKO mice. As seen in our previous studies, development of AHR was reduced in SEA-challenged IL-10$^{-/-}$ mice (Figure 5A). In contrast, the AHR responses in dKO mice were significantly exacerbated when compared with those in either WT or IL-10$^{-/-}$ mice. The difference between the IL-10$^{-/-}$ and dKO mice was particularly striking. Thus, these data identify IL-13Rα2 as a critical regulator of AHR in IL-10$^{-/-}$ mice. Nevertheless, to further investigate the importance of IL-13Rα2, we also examined whether restoring decoy receptor activity in the dKO mice could reverse their exacerbated AHR. To do this, we treated additional dKO mice with soluble IL-13Ra2-Fc fusion protein (sIL-13Ra2-Fc) prior to allergen challenge and compared the development of AHR with that in untreated IL-10$^{-/-}$ and dKO mice. As predicted, the sIL-13Rα2-Fc–treated dKO mice developed weak AHR responses that were now nearly identical to those of IL-10$^{-/-}$ mice, thus confirming an important inhibitory role for IL-13Rα2 (Figure 5A). We also confirmed the inhibitory role of IL-13Rα2 in IL-10$^{-/-}$ mice by assessing AHR using direct invasive assays of lung resistance (R_L) in mice that were anesthetized, tracheostomized, and mechanically ventilated

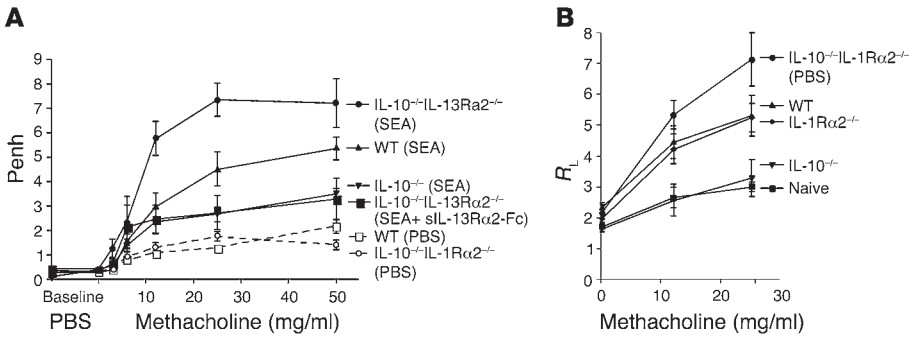

Figure 5
Removing IL-13Rα2 in IL-10$^{-/-}$ mice reveals a role for IL-13Rα2 in controlling AHR. Animals were sensitized and challenged as in Figure 1. Animals were euthanized 24 hours after the final airway challenge. (**A**) AHR. Penh measurements 24 hours after the final airway challenge using a Buxco system with mice exposed to increasing doses of methacholine. Results from 1 of 3 representative experiments are shown. (**B**) AHR. R_L measurements 24 hours after the final airway challenge with mice exposed to increasing doses of methacholine. Results from 1 of 2 representative experiments are shown.

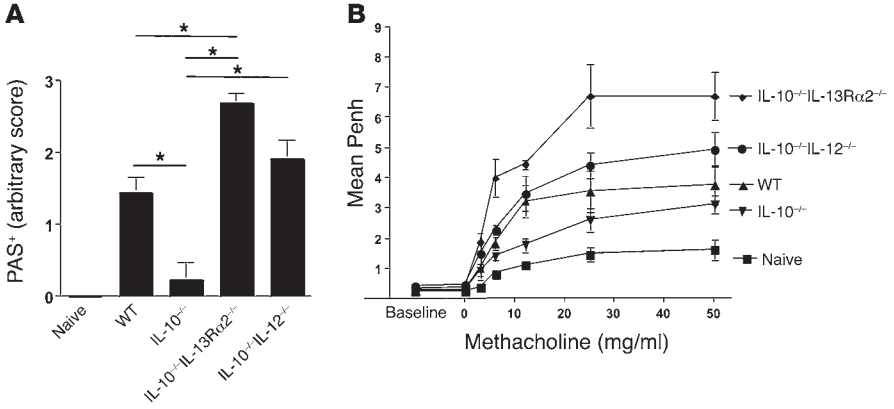

Figure 6
Both IL-12 and IL-13Rα2 regulate AHR and goblet cell hyperplasia in the absence of IL-10. Animals were sensitized and challenged as in Figure 1. *$P < 0.05$, 1-way ANOVA. (**A**) Five-micrometer sections were cut from paraffin-embedded lung tissue and stained with alcian blue–PAS. Five lungs from each group were scored in a blinded fashion. (**B**) AHR. Penh measurements 24 hours after the final airway challenge using a Buxco system with mice exposed to increasing doses of methacholine. Results from 1 of 2 representative experiments are shown.

(Figure 5B). Here again, the dKO mice developed the most severe AHR, while allergen-challenged IL-10$^{-/-}$ mice displayed responses that were barely increased above baseline.

The inhibitory effects of IL-13Rα2 are superior to the Th1 response. In addition to the elevated IL-13Rα2 response, IL-10$^{-/-}$ mice also exhibited a significant increase in cells capable of secreting IFN-γ (Figure 3F). Because IL-12 and IFN-γ are known to inhibit mucus production in the lung (41, 42), we also investigated whether the Th1 response was contributing to the suppression of mucus and AHR in IL-10$^{-/-}$ mice. To do this, we bred BALB/c IL-10$^{-/-}$ mice with IL-12p40$^{-/-}$ mice to generate IL-10$^{-/-}$IL-12$^{-/-}$ mice and compared their allergen-induced mucus and AHR responses with those of WT, IL-10$^{-/-}$, and IL-10$^{-/-}$IL-13Rα2$^{-/-}$ dKO mice. As expected, the mucus response in IL-10$^{-/-}$ mice was significantly reduced compared with that in WT animals (Figure 6A). However, the simultaneous deletion of IL-10 and IL-12 restored the mucus response back to WT levels, indicating that IL-12 was at least partly contributing to the suppression of mucus production in IL-10$^{-/-}$ mice. Nevertheless, the mucus response in the IL-10$^{-/-}$IL-13Rα2$^{-/-}$ mice was even more marked (Figure 6A), despite the fact that they generated IFN-γ responses comparable to those of IL-10$^{-/-}$ mice (Figure 3F). These observations suggest that IL-13Rα2 deficiency can supersede the suppressive effects of IL-12/IFN-γ. A similar pattern emerged when their AHR responses were measured (Figure 6B). Here again, although the AHR response of IL-10$^{-/-}$IL-12$^{-/-}$ mice was significantly elevated relative to that of IL-10$^{-/-}$ mice, the increase observed in IL-10$^{-/-}$IL-13Rα2$^{-/-}$ mice was much more dramatic, adding further weight to the importance of the IL-13 decoy receptor.

Chronic Th2 responses are defined by persistent IL-10 and IL-13Rα2 production. Having established distinct roles for IL-10 and IL-13Rα2 in an acute model of Th2-mediated allergy, we next asked whether IL-10 and IL-13Rα2 regulate chronic Th2 responses. For these studies, we used the infectious trematode *S. mansoni*, which induces a chronic Th2-dominant inflammatory response. In this model, schistosome eggs are deposited in the liver, inducing a fibrotic granulomatous response. IL-10 and IL-13Rα2 expression was monitored throughout infection using IL-10–GFP reporter mice infected with 30 *S. mansoni* cercariae. The dominant population of IL-10^{+} cells in the liver (Figure 7A), spleen (data not shown), and mesenteric lymph nodes (data not shown) expressed CD4 and CD25 and likely represent IL-10–producing regulatory T cells (27). The serum IL-13Rα2 response was strikingly similar to the IL-10 response (Figure 7B), increasing 2- to 3-fold at the acute stage (week 8) and remaining elevated in chronically infected mice (week 16). Infection of IL-10$^{-/-}$ mice led to elevated serum IL-13Rα2 compared with WT mice (Figure 7C), similar to our allergen-challenged IL-10$^{-/-}$ mice (Figure 2G), although the difference was not significant in this case. The increase

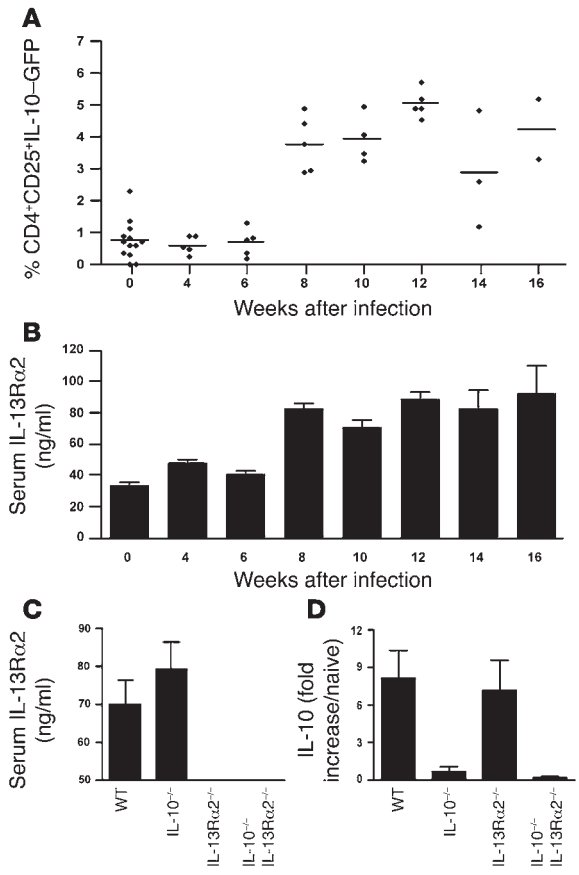

Figure 7
Recruitment of IL-10–GFP^{+}CD4^{+}CD25^{+} cells into the liver and increased serum IL-13Rα2 following infection with *S. mansoni*. IL-10–GFP reporter (tiger) mice were infected with 30 *S. mansoni* cercariae and euthanized on indicated weeks after infection. (**A**) Livers were excised from infected IL-10–GFP reporter mice on the indicated weeks after infection. Tissues were prepared into a single-cell suspension and stained with fluorescently labeled antibody anti-CD4 (APC) and anti-CD25 (PE). (**B** and **C**) Serum IL-13Rα2 was measured by ELISA. (**D**) RNA was extracted from liver tissue, with IL-10 mRNA quantified by qRT-PCR.

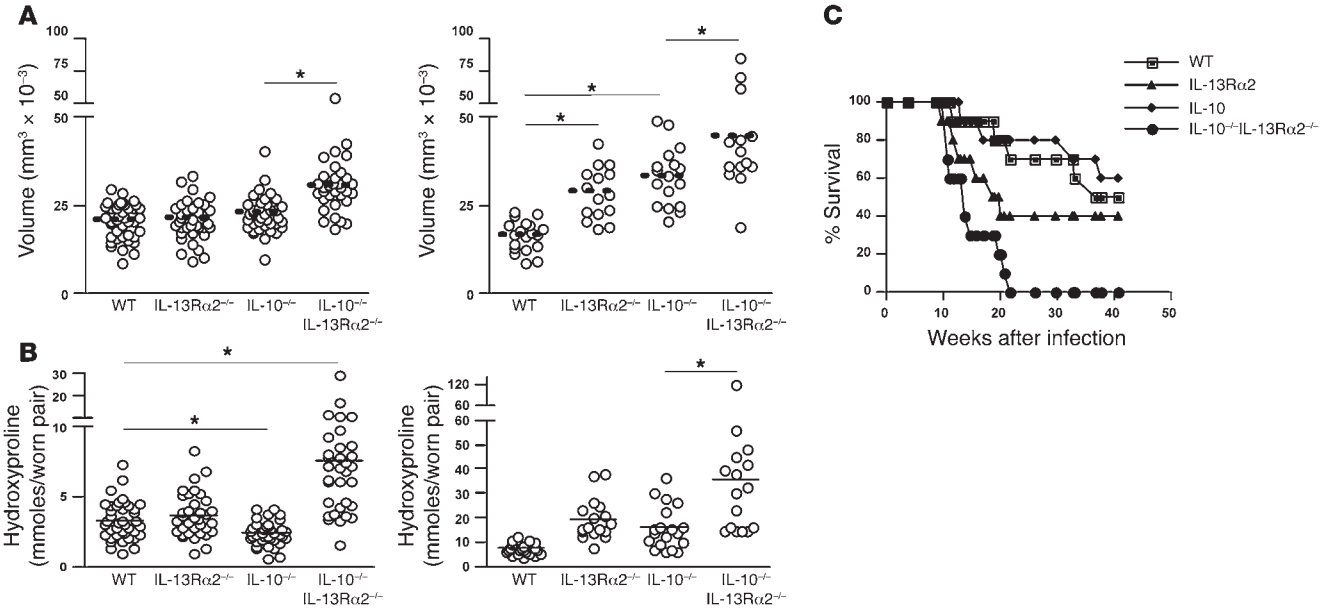

Figure 8

Increased granuloma volume and fibrosis in IL-10$^{-/-}$IL-13Rα2$^{-/-}$ dKO mice. Mice were infected with 30 *S. mansoni* cercariae and euthanized at week 8 (early) and week 12 (late) during the chronic stages of egg-induced pathology. *$P < 0.05$, Mann-Whitney *U* test for single comparisons or 1-way ANOVA for multiple comparisons. Similar numbers of paired adult parasites and eggs were found in the tissues of all groups, so the observed pathological changes were not attributed to differences in parasite burden. (**A**) Liver tissue was excised, fixed, sectioned, and stained with Wright-Giemsa. Granuloma volume was calculated in a blinded fashion from Giemsa-stained liver sections at weeks 8 (left) and 12 (right) after infection. (**B**) Liver fibrosis (μmol of hydroxyproline per worm pair) was calculated from liver biopsies taken at weeks 8 (left) and 12 (right) after infection. (**C**) A survival study was conducted with mice infected with 30 *S. mansoni* cercariae.

in IL-10 mRNA expression observed in infected WT mice was also not significantly affected by IL-13Rα2 deficiency (Figure 7D), suggesting that IL-10 and IL-13Rα2 are induced and regulated independently during infection with *S. mansoni*.

Granuloma formation and fibrosis are suppressed by the combined actions of IL-10 and IL-13Rα2. To investigate the functional role of IL-10 and IL-13Rα2 in a chronic Th2 disease setting, mice were infected with 30 cercariae, and granuloma formation and fibrosis were assessed at 8 and 12 weeks after infection. At week 8, deletion of IL-13Rα2 or IL-10 had no impact on granuloma size (Figure 8A, left) or cellular composition (data not shown). However, granuloma size was exacerbated in the dKO mice (30% increase versus WT), demonstrating that IL-10 and IL-13Rα2 function as cooperative inhibitors of granulomatous inflammation, at least during the acute phase of infection. By week 12, IL-10$^{-/-}$ and IL-13Rα2$^{-/-}$ mice also displayed significantly larger granulomas (Figure 8A, right). Indeed, while WT mice displayed a 20% decrease in granuloma size between weeks 8 and 12, IL-10$^{-/-}$ and IL-13Rα2$^{-/-}$ mice exhibited significantly larger granulomas at the chronic time point. Strikingly, the granulomas in dKO mice were approximately 50% larger than those in WT animals on week 12 and 20%–30% larger than those in the single-KO mice. Thus, these data demonstrate that chronic Th2-mediated inflammation is downmodulated by the combined actions of IL-10 and IL-13Rα2.

In contrast to granuloma size, which is downmodulated in chronically infected WT animals, liver fibrosis steadily increases as long as the animals remain infected. Therefore, we examined whether IL-10 and IL-13Rα2 regulated the progression of liver fibrosis by measuring hydroxyproline content and staining liver sections with picrosirius red. On week 8, liver fibrosis was similar in WT and IL-13Rα2$^{-/-}$ mice, but significantly decreased in IL-10$^{-/-}$ mice (Figure 8B, right). Interestingly, the decreased fibrotic response in IL-10$^{-/-}$ mice was consistent with their reduced AHR following SEA challenge in the lung (Figure 2D). In both settings, the reduced pathological responses were associated with significant IL-13Rα2 expression (Figure 2F and Figure 7C). Thus, despite displaying either similar or increased inflammation, many other pathological features were reduced in the IL-10$^{-/-}$ mice. The important contribution of IL-13Rα2 was again revealed in the dKO mice, which in contrast to IL-10$^{-/-}$ mice developed exacerbated liver fibrosis by week 8, mirroring the exacerbated AHR and mucus responses observed in our lung studies. Thus, deleting IL-13Rα2 on an IL-10$^{-/-}$ background completely reversed the pathological phenotype of the IL-10$^{-/-}$ mice. The combined antifibrotic activities of IL-10 and IL-13Rα2 were particularly evident at the chronic time point. Indeed, by week 12, both of the single-KO groups were now displaying significant increases in fibrosis (Figure 8B). Nevertheless, the dKO mice again displayed the most dramatic increase, with liver fibrosis nearly doubling in the dKO mice when compared with 12-week-infected WT, IL-10$^{-/-}$, or IL-13Rα2$^{-/-}$ mice (Figure 8B, left).

IL-13 effector function is enhanced in IL-10/IL-13Rα2 dKO mice. Granuloma formation and fibrosis are regulated by the egg-induced IL-13 response. To determine whether local changes in Th2 effector function were responsible for the exacerbated fibrotic responses in the dKO mice, liver RNA was isolated from infected mice and examined by real-time PCR (Supplemental Figure 3). As expected, there were marked increases in IL-13 and IL-5 mRNA in the livers of infected WT mice. However, there were no significant differences in the IL-10$^{-/-}$ and IL-13Rα2$^{-/-}$ mice, suggesting relatively little effect

on Th2 response development in vivo (Supplemental Figure 3, A and E). Nevertheless, when the expression of several Th2-regulated genes was examined, it was clear that IL-10 and IL-13Rα2 were playing distinct roles in the regulation of Th2 effector function. Three distinct subsets of genes were analyzed, including markers of alternative macrophage activation (Ym1 and FIZZ1), MMPs (MMP-9 and MMP-12), and interstitial collagens (COL III and COL VI), all linked with Th2 effector function (43, 44). Interestingly, deletion of IL-10 alone had little effect. Indeed, only small increases in MMP-12 and minor reductions in pro-Col III and pro-Col VI mRNA were observed in IL-10$^{-/-}$ mice (Supplemental Figure 3), consistent with their suppressed fibrotic responses at 8 weeks after infection (Figure 8B). However, deleting IL-13Rα2 alone or in combination with IL-10 led to significantly increased Ym-1, FIZZ-1, MMP-9, MMP-12, pro-Col III, and pro-Col VI mRNA expression when compared with WT mice (Supplemental Figure 3). These data suggest that IL-13Rα2 is the dominant regulator of IL-13 effector function in the tissues. In fact, the only difference detected between IL-13Rα2$^{-/-}$ and dKO mice was a slight increase in Ym-1 and MMP-9 and small but significant increase in MMP-12 and IL-5 in the dKO mice. Thus, although it is clear that IL-10 and IL-13Rα2 both regulate Th2-driven disease, they target distinct pathological features, with IL-10 inhibiting inflammation and IL-13Rα2 suppressing downstream IL-13–dependent effector responses (AHR/mucus/tissue remodeling/fibrosis).

IL-10 and IL-13Rα2 collaborate to control mortality following infection with S. mansoni. Finally, survival studies were performed with the various KO mice for up to 42 weeks to determine the long-term consequences of IL-10/IL-13Rα2 deficiency. Deletion of IL-10 alone had little impact on survival, with 80% survival at week 20 (Figure 8C). In contrast, IL-13Rα2$^{-/-}$ mice displayed significant mortality, with only 40% of the animals surviving through week 20. dKO mice, however, had the most dramatic response, with 40% mortality observed as early as week 10 after infection and reaching nearly 100% by week 20. In most cases, blood was found in the gut at autopsy. These data demonstrate that survival during *S. mansoni* infection is controlled by IL-10 and IL-13Rα2. Nevertheless, the results suggest that IL-13Rα2 plays the greater role during chronic Th2-driven responses.

Discussion

Diseases characterized by persistent Th2 cytokine responses, such as asthma and chronic helminth infections, are associated with the development of significant tissue pathology. Recent studies established a critical role for IL-13 in these processes (3). Although IL-10 has been shown to regulate Th2-driven inflammation, we show that many of the pathological changes associated with persistent Th2 responses are inhibited by the actions of the IL-13 decoy receptor IL-13Rα2. IL-10 and IL-13Rα2 were both upregulated during acute and chronic Th2 responses, and mice genetically deficient in IL-10 and IL-13Rα2 (dKO mice) developed exacerbated pathology. In contrast to IL-10$^{-/-}$ mice, the dKO mice developed significant AHR and goblet cell hyperplasia following allergen exposure in the lung. The dKO mice also developed more fibrosis during acute *S. mansoni* infection, compared with IL-10$^{-/-}$ mice, and they rapidly succumbed to the infection. Thus, IL-10 and IL-13Rα2 are both required to restrain Th2-dependent inflammation and to prevent development of downstream immunopathologies. Indeed, our data illustrate distinct but cooperative roles for IL-10 and IL-13Rα2 in the downregulation of Th2-driven pathology.

The function of IL-10 in Th2 immunity is controversial, with reports arguing for and against a role for IL-10 in the development of Th2 responses and associated pathologies (28). For example, transgenic expression of IL-10 in the airways exacerbated silica-induced Th2 pathology (29), with IL-10 overexpression triggering mucus metaplasia, tissue inflammation, and airway remodeling (45). However, other studies suggested that IL-10 is either not involved in (24, 38) or has an inhibitory effect on Th2 responses (31, 33). Indeed, it has previously been shown that IL-10 (33, 34) or IL-10–producing CD4$^+$CD25$^+$ cells can inhibit Th2-associated airway inflammation (35, 36) as well as granuloma formation in schistosomiasis (27). Our data support an inhibitory role for IL-10, since IL-10$^{-/-}$ mice displayed significantly stronger Th2 responses following allergen exposure in the lung or when infected with *S. mansoni*. Nevertheless, despite developing stronger Th2 responses and increased inflammation, several pathological features associated with IL-13 production were reduced in the absence of IL-10. The explanation for these divergent findings was unknown, although they indicated that additional mechanisms were regulating Th2 effector function.

Several studies have reported a failure to induce AHR in IL-10$^{-/-}$ mice, an IL-13–driven process (11), even though IL-10$^{-/-}$ mice develop stronger Th2 responses and increased inflammation (37, 38). Previous studies suggested that IL-10 acts directly on airway smooth muscle cells and is thus critically involved in the development of AHR. In support of these findings, a study by Van Scott and colleagues (33) observed increased AHR following IL-10 administration, despite significantly reduced inflammation. We observed a similar paradoxical role for IL-10 in our studies, with increased inflammation and IL-13 production in IL-10$^{-/-}$ mice correlating with reduced AHR. The decrease in AHR was also associated with reduced mucus production and *gob 5* and *Muc5ac* mRNA expression in the lung, suggesting that IL-13 bioactivity was being inhibited in the absence of IL-10 (46). Interestingly, IL-13Rα2 mRNA expression increased in the lungs of the IL-10$^{-/-}$ mice, and elevated levels of the soluble IL-13Rα2 were found in the serum. Therefore, we theorized that the IL-13 decoy receptor, produced primarily by activated fibroblasts and epithelial cells (18, 47–49), might be responsible for the reduced AHR and mucus responses of allergen-challenged IL-10$^{-/-}$ mice.

To formally test this hypothesis, we generated IL-10$^{-/-}$IL-13Rα2$^{-/-}$ (dKO) mice and compared their responses with those of IL-10$^{-/-}$ and IL-13Rα2$^{-/-}$ mice in acute and chronic Th2 models. Strikingly, although inflammation was similarly increased in IL-10$^{-/-}$ and dKO mice following intratracheal SEA administration, the reduced AHR and mucus responses of IL-10$^{-/-}$ mice were completely reversed in the dKO animals. In fact, the dKO mice developed stronger AHR when compared with both IL-10$^{-/-}$ and WT mice, suggesting that IL-13Rα2 was functioning as a potent negative regulator of AHR, particularly in IL-10$^{-/-}$ mice, which develop stronger Th2 responses. Consequently, these observations rule out IL-10 as a direct inducer of AHR (37, 38). We were also able to reverse the phenotype of the dKO mice by administering a soluble form of IL-13Rα2 (sIL-13Rα2-Fc) (14, 16, 18), thus further demonstrating the critical role of the IL-13 decoy receptor in the suppression of AHR. Although previous studies utilized sIL-13Rα2-Fc to neutralize IL-13 function (50–53), to our knowledge these are the first data demonstrating an important functional role for the endogenous IL-13Rα2 in a model of allergic airway inflammation. They also reveal an essential collaboration between IL-10 and IL-13Rα2, with IL-10 functioning as the dominant inhibitor of inflammation and Th2 cytokine production and IL-13Rα2 serving as a key downstream inhibitor of AHR and mucus secretion.

Mechanistically, these data argue that IL-13Rα2 is responsible for the reduced AHR and mucus responses of IL-10$^{-/-}$ mice. However,

in addition to generating stronger IL-13Rα2 responses, the IL-10$^{-/-}$ mice also displayed significant increases in IL-12 (data not shown) and IFN-γ, both of which have been shown to antagonize goblet cell hyperplasia (54, 55). Thus, increased production of Th1 cytokines could provide an additional explanation for the reduced mucus and AHR responses of IL-10$^{-/-}$ mice. In contrast to their effects on goblet cell hyperplasia, however, the role of IFN-γ and IL-12 in the regulation of AHR is more controversial, with some reports demonstrating a reduction in AHR following exogenous IFN-γ/IL-12 treatment (41, 42) and others showing a reduction when the cytokines are blocked (55). Therefore, to clarify the potential contribution of the elevated Th1 response of IL-10$^{-/-}$ mice, we also generated IL-10$^{-/-}$IL-12$^{-/-}$ mice and compared their AHR and mucus responses with those of the IL-10$^{-/-}$ and IL-10$^{-/-}$IL-13Rα2$^{-/-}$ animals. Although deletion of IL-12 on the IL-10$^{-/-}$ background led to significant increases in AHR and goblet cell hyperplasia, the responses in IL-10$^{-/-}$IL-13Rα2$^{-/-}$ dKO mice were consistently more marked, suggesting that IL-13Rα2 was functioning as the dominant inhibitor. When viewed together, these data demonstrate that the IL-13 decoy receptor and Th1 response cooperate to suppress AHR and mucus production in IL-10$^{-/-}$ mice. Thus, it will be important to determine whether similar mechanisms are at play in humans suffering from various Th2-associated disorders.

The studies conducted in the lung focused on the role of IL-10 and IL-13Rα2 in an acute setting of Th2-driven disease. Therefore, we performed additional studies with the schistosomiasis model, a well-established system for studying chronic Th2-driven inflammation. Similar to our lung studies, granulomatous inflammation increased in the IL-10$^{-/-}$ mice, compared with WT mice, particularly at the acute time point after infection (week 8). The increase in granuloma size was also associated with a marked increase in Th2 cytokine production in the liver. Nevertheless, fibrosis and pro-Col III and pro-Col VI mRNA expression were significantly reduced in the IL-10$^{-/-}$ mice at week 8. As in the lung, the decrease in liver fibrosis was associated with a significant IL-13Rα2 response. Importantly, infection studies conducted with dKO mice revealed the critical regulatory function of IL-13Rα2. Here again, acute inflammation was predominantly controlled by IL-10, while IL-13Rα2 served as the dominant inhibitor of fibrosis. Indeed, IL-10$^{-/-}$ and dKO mice displayed a similar increase in granulomatous inflammation at week 8. However, fibrosis was enhanced only in dKO mice and associated with enhanced MMP9, pro-Col III, and pro-Col VI mRNA expression compared with that in IL-10$^{-/-}$ mice.

The cooperation between IL-10 and IL-13Rα2 was particularly evident in chronically infected mice, where IL-10 and IL-13Rα2 have previously been shown independently to downregulate granulomatous inflammation and fibrosis (27, 56, 57). Nevertheless, the dKO mice consistently developed the largest granulomas and most severe liver fibrosis, which likely contributed to their accelerated mortality. Thus, these data suggest that 2 distinct but equally important regulatory molecules inhibit acute and chronic Th2 pathologies. Their mechanisms of action appear to be unique, with IL-10 controlling CD4$^+$ Th2 cell development and inflammation and IL-13Rα2 regulating IL-13 effector function, including AHR, mucus secretion, and fibrosis. These findings likely explain the confusing literature regarding the function of IL-10 in Th2 immunity, since few studies have considered the important contribution of the IL-13 decoy receptor. From this study, it is clear that Th2-mediated inflammation does not always correlate with the development of significant immunopathology and that targeting specific mediators, such as IL-13, may curtail or even prevent immune-mediated pathologies while allowing inflammation to continue. They also illustrate how IL-10 and IL-13Rα2 might be exploited in the treatment of a variety of Th2-driven diseases, including asthma, ulcerative colitis, and chronic helminth infections.

Methods

Animals. Female BALB/c, C57BL/6, BALB/c IL-13Rα2$^{-/-}$, BALB/c IL-10$^{-/-}$, BALB/c IL-10$^{-/-}$IL-13Rα2$^{-/-}$ (BALB/c background; ≥10 generations) and BALB/c IL-10$^{-/-}$IL-12$^{-/-}$ (BALB/c background; ≥10 generations), 6–8 weeks old, were obtained from NIAID animal facilities at Taconic. IL-10-GFP reporter mice, designated as tiger (interleukin-ten ires GFP-enhanced reporter), were generated at the Yale University School of Medicine as described previously (40) and bred as homozygotes for the transgene. All animals were housed under specific pathogen–free conditions at the NIH in an American Association for the Accreditation of Laboratory Animal Care–approved facility. The NIAID animal care and use committee approved all experimental procedures. A minimum of 5 mice per group were used in each experiment, unless otherwise indicated.

Reagents. *S. mansoni* SEA was obtained from sterile LPS-free liver-derived eggs from chronically infected BALB/c mice.

Allergen-induced airway inflammation. Mice were immunized by i.p. inoculation with 10 μg SEA from *S. mansoni* in PBS and boosted again with 10 μg of SEA i.p. 14 days later. On days 28 and 31, mice were anesthetized with 20 μl/g body weight i.p. of a tribromoethanol anesthetic, Avertin, and given airway challenges with 10 μg of SEA in PBS by the intratracheal route. Mice were killed 24 hours after the final airway challenge (day 32) to assess airway inflammation and AHR.

S. mansoni infection. Mice were infected percutaneously via the tail with 30 cercariae of a Puerto Rican strain of *S. mansoni* (NMRI) obtained from *Biomphalria glabrata* snails (Biomedical Research Institute). SEA was obtained from purified and homogenized *S. mansoni* eggs as described previously (58). Animals were perfused at the time of euthanasia so that worm and tissue egg burdens could be determined as described previously (58).

BAL fluid and differential cell counts. Twenty-four hours after the final challenge, mice were anesthetized with pentobarbital. The trachea was cannulated and airspaces lavaged with an initial 500 μl of sterile PBS, followed by two 500-μl PBS washes. Fluids were centrifuged at 1,200 *g*, and pellets recovered from all 3 lavage washes were pooled into 1 ml of PBS for total BAL cell counts and cellular analysis. The supernatants of the initial 500 μl of BAL fluid were stored at –80°C for biochemical analyses. Cytospins were prepared by spinning 5×10^5 cells onto poly-(L-lysine)–coated slides followed by Diff-Quick (Boehringer) staining. Differential cell counts were performed at ×100 magnification; a minimum of 200 cells were counted for each slide.

AHR. Mean Penh was calculated from a 5-minute measurement period after administration of 2.5 minutes of inhaled methacholine (Sigma-Aldrich) at 3–50 mg/ml. Penh measurements were executed 24 hours after the final SEA challenge by whole-body plethysmography (Buxco) as described previously (59). For measurement of intubated R_L, mice were anesthetized with sodium pentobarbital on day 32, one day after last SEA challenge. Mice were mechanically ventilated at a rate of 150 breaths/min with a tidal volume of 6 ml/kg. One port of a 4-way connector was attached to the tracheotomy tube, and the other 2 ports were attached to the inspiratory and expiratory side of the ventilator, respectively. Aerosolized methacholine was administered for 10 seconds with a tidal volume of 10 μl, with airflow calculated from the pressure changes of the plethysmograph by BioSystem XA software (Buxco). Mean R_L was registered continuously during the infusion of methacholine to express changes in murine airway function as previously described (60).

ELISA. Cytokines were measured by ELISA using suppliers' guidelines. Capture antibodies for IL-5 (2 μg/ml) were from BD Biosciences — Pharmingen. Capture antibodies for eotaxin (0.4 μg/ml) were from

R&D Systems. Biotinylated detection antibodies were from BD Biosciences — Pharmingen (IL-5; 2 μg/ml) or R&D Systems (eotaxin; 0.4 μg/ml). In vivo serum IL-5 was measured according to ref. 61. Total IgE was measured with anti-mouse IgE capture antibody (clone R35-72; BD Biosciences — Pharmingen) and biotinylated anti-mouse IgE detection antibody (clone R35-118; BD Biosciences — Pharmingen), using a monoclonal IgE standard curve (clone 27-74; catalog 553481). To measure soluble IL-13Rα2, immunosorbent plates were coated with rmIL-13 (0.5 μg/ml) (provided by Wyeth) in PBS overnight. Plates were washed with 0.05% Tween-20 in PBS (PBST) and blocked with 5% milk in PBST. Mouse serum (at 1:10 or 1:40) and assay standard diluted in PBST plus 1% BSA were added for 2 hours at 37°C. The detection antibody biotinylated goat anti-mouse IL-13Rα2 (R&D Systems) was added for 2 hours at 37°C. Peroxidase-labeled streptavidin (1:1,000 for 1 hour at 37°C) and ABTS (2,2′-azino-di[3-ethylbenzthiazoline-6-sulfonate]) peroxidase substrate (both from Kirkegaard & Perry Laboratories) were used to detect biotinylated antibody. The concentration of IL-13Rα2 in the sample was determined from a serial-fold diluted standard of rmIL-13Rα2-Fc/chimera (R&D Systems). The sensitivity of the assay was 98 pg/ml. OD was read at 405 nm in an ELISA reader.

Flow cytometry. Cells were stained with antibodies diluted in PBS with 0.5% BSA (Sigma-Aldrich), 0.05% sodium azide (Sigma-Aldrich) for 20 minutes at 4°C. For detection of $CD4^+CD25^+$IL-10–GFP^+ cells, monoclonal rat anti-mouse CD4 (L3T4, clone RM4-5, isotype rat IgG2a) and rat anti-mouse CD25 (PC61, isotype rat IgG1) were used. For detection of intracellular IL-13 and IFN-γ, cells were stimulated with PMA and ionomycin in the presence of brefeldin A for 3 hours, after which cells were surface stained for CD4 and/or CD25, permeabilized in Cytofix/Cytoperm (BD Biosciences — Pharmingen), washed in Perm/Wash buffer (BD Biosciences — Pharmingen) according to the manufacturer's recommendations, and stained with PE-labeled rat anti-mouse IL-13 (unlabeled antibody provided by Lily Li, Centocor, Horsham, Pennsylvania, USA) or FITC-labeled anti-mouse IFN-γ (BD Biosciences — Pharmingen) for 30 minutes. IL-10–GFP reporter mice, designated as tiger, allowed us to identify IL-10–producing cells ex vivo without subsequent manipulation. The expression of surface markers and intracellular cytokines was analyzed on a FACSCalibur (BD) flow cytometer using FlowJo software (Tree Star).

Histopathology and fibrosis. The sizes of hepatic granulomas were determined on histological sections stained with Wright-Giemsa stain. Around 30 granulomas per mouse were included in all analyses. Hepatic collagen was measured as hydroxyproline after hydrolysis of 200 mg of liver in 5 ml of 6 N HCl. The increase in hepatic hydroxyproline was positively related to worm pairs in all experiments and was expressed as micromoles per worm pair ([infected liver collagen – normal liver collagen]/worm pair). The same individual scored all histological features and had no knowledge of the experimental design. For histopathological analyses of lungs in the allergy model, formalin-fixed (4% paraformaldehyde in PBS) lungs were processed and embedded in paraffin for sectioning (Histopath of America). H&E stains or Giemsa stains were used for analysis of airway inflammation and pathological changes. Perivascular and peribronchial inflammation as well as edema evaluations were scored on a scale of 1–4+ arbitrary units by an observer blinded to the experimental protocol, taking into account both the degree of inflammation and its distribution. For example, an inflammatory infiltrate would be graded as 3+ if an infiltrate of 4 cells in thickness involved most bronchi and blood vessels. The sum of both scores was used to quantify inflammation (up to a total of 8+). Goblet cells were stained with alcian blue–PAS (AB-PAS) with positive bronchial epithelial cells also scored on an arbitrary 1–4+ basis. PAS-positive cells were confined to bronchi more than 100 μm in diameter. A 3+ grade was given when a third of the cells in most bronchi more than 100 μm in diameter were positive, a 1+ grade when more than 10 cells in such bronchi were found in the section.

RNA isolation and purification and real-time PCR. Total RNA was extracted from lung and liver tissue samples in 1 ml TRIzol reagent (Invitrogen). The sample was homogenized using a tissue Polytron (Omni International), and total RNA was extracted according to the recommendations of the manufacturer and further purified using an RNeasy Mini Kit from QIAGEN. Individual sample RNA (1 μg) was reverse transcribed using SuperScript II Reverse Transcriptase (Invitrogen) and a mixture of oligo(dT) and random primers. Real-time RT-PCR was performed on an ABI Prism 7900HT Sequence Detection System (Applied Biosystems). Relative quantities of mRNA for several genes was determined using SYBR Green PCR Master Mix (Applied Biosystems) and by the comparative threshold cycle method as described by Applied Biosystems for the ABI Prism 7700/7900HT Sequence Detection Systems. In this method, mRNA levels for each sample were normalized to hypoxanthine guanine phosphoribosyl transferase (HPRT) mRNA levels and then expressed as a relative increase or decrease compared with levels in uninfected controls. Primers were designed using Primer Express software (version 2.0; Applied Biosystems). Primers for IL-4, IL-13, IL-10, HPRT, IL-13Rα2, Ym-1, Fizz-1, and IFN-γ were previously published in ref. 62. Other primer sequences were as follows: IL-5, sense 5′-TGACAAGCAATGAGACGATGAGG-3′, antisense 5′-ACCCCCACGGACAGTTTGATTC-3′; *gob 5*, sense 5′-CATCGCCATAGACCACGACG-3′, antisense 5′-TTCCAGCTCTCGGGAATCAAA-3′; *Muc5ac*, sense 5′-CAGGACTCTCTGAAATCGTACCA-3′, antisense 5′-AAGGCTCGTACCACAGGGA-3′; COL III, sense 5′-AACCTGGTTTCTTCTCACCCTTC-3′, antisense 5′-ACTCATAGGACTGACCAAGGTGG-3′; COL VI, sense 5′-CGCCCTTCCCACTGACAA-3′, antisense 5′-GCGTTCCCTTTAAGACAGTTGAG-3′; MMP-9, sense 5′-CAGACGTGGGTCGATTCCA-3′, antisense 5′-CATCTCTCGCGGCAAGTCTT-3′; MMP-12, sense 5′-CTGGGCAACTGGACAACTCAACTC-3′, antisense 5′-AATGCTGCAGCCCCAAGGAAT-3′.

Statistics. Data sets were compared by Mann Whitney *U* test or 1-way ANOVA as specified in figure legends. Differences were considered significant at $P < 0.05$.

Acknowledgments

The authors acknowledge the meticulous care of animals used in this study by Jason Clardy and colleagues (SoBran Inc.). We thank Fred Lewis and colleagues (Biomedical Research Institute) for schistosome material and Satish Madala and Vergilio Bundoc for technical help. We also thank Michael Grusby and Wyeth Research for providing the original breeding pairs of IL-13Rα2–deficient mice. This research was supported by the Intramural Research Program of the NIH, NIAID.

Received for publication January 18, 2007, and accepted in revised form July 6, 2007.

Address correspondence to: Thomas A. Wynn, Immunopathogenesis Section, Laboratory of Parasitic Diseases, National Institute of Allergy and Infectious Diseases, NIH, 50 South Drive, Room 6154, Bethesda, Maryland 20892, USA. Phone: (301) 594-4758; Fax: (301) 480-5025; E-mail: twynn@niaid.nih.gov.

1. Wills-Karp, M. 1999. Immunologic basis of antigen-induced airway hyperresponsiveness. *Annu. Rev. Immunol.* **17**:255–281.
2. Sher, A., and Coffman, R.L. 1992. Regulation of immunity to parasites by T cells and T cell-derived cytokines. *Annu. Rev. Immunol.* **10**:385–409.
3. Wynn, T.A. 2003. IL-13 effector functions. *Annu. Rev. Immunol.* **21**:425–456.
4. Huang, S.K., et al. 1995. IL-13 expression at the sites of allergen challenge in patients with asthma. *J. Immunol.* **155**:2688–2694.
5. Wills-Karp, M., et al. 1998. Interleukin-13: central

mediator of allergic asthma. *Science.* **282**:2258–2261.
6. Grunig, G., et al. 1998. Requirement for IL-13 independently of IL-4 in experimental asthma. *Science.* **282**:2261–2263.
7. Zhu, Z., et al. 1999. Pulmonary expression of interleukin-13 causes inflammation, mucus hypersecretion, subepithelial fibrosis, physiologic abnormalities, and eotaxin production. *J. Clin. Invest.* **103**:779–788.
8. Zhu, Z., et al. 2002. IL-13-induced chemokine responses in the lung: role of CCR2 in the pathogenesis of IL-13-induced inflammation and remodeling. *J. Immunol.* **168**:2953–2962.
9. Bochner, B.S., et al. 1995. IL-13 selectively induces vascular cell adhesion molecule-1 expression in human endothelial cells. *J. Immunol.* **154**:799–803.
10. Venkayya, R., et al. 2002. The Th2 lymphocyte products IL-4 and IL-13 rapidly induce airway hyperresponsiveness through direct effects on resident airway cells. *Am. J. Respir. Cell Mol. Biol.* **26**:202–208.
11. Yang, M., et al. 2001. Interleukin-13 mediates airways hyperreactivity through the IL-4 receptor-alpha chain and STAT-6 independently of IL-5 and eotaxin. *Am. J. Respir. Cell Mol. Biol.* **25**:522–530.
12. Vasakova, M., et al. 2006. Th1/Th2 cytokine gene polymorphisms in patients with idiopathic pulmonary fibrosis. *Tissue Antigens.* **67**:229–232.
13. Heller, F., et al. 2005. Interleukin-13 is the key effector Th2 cytokine in ulcerative colitis that affects epithelial tight junctions, apoptosis, and cell restitution. *Gastroenterology.* **129**:550–564.
14. Chiaramonte, M.G., Donaldson, D.D., Cheever, A.W., and Wynn, T.A. 1999. An IL-13 inhibitor blocks the development of hepatic fibrosis during a T-helper type 2-dominated inflammatory response. *J. Clin. Invest.* **104**:777–785.
15. McDermott, J.R., Humphreys, N.E., Forman, S.P., Donaldson, D.D., and Grencis, R.K. 2005. Intraepithelial NK cell-derived IL-13 induces intestinal pathology associated with nematode infection. *J. Immunol.* **175**:3207–3213.
16. Donaldson, D.D., et al. 1998. The murine IL-13 receptor alpha 2: molecular cloning, characterization, and comparison with murine IL-13 receptor alpha 1. *J. Immunol.* **161**:2317–2324.
17. Wood, N., et al. 2003. Enhanced interleukin (IL)-13 responses in mice lacking IL-13 receptor alpha 2. *J. Exp. Med.* **197**:703–709.
18. Chiaramonte, M.G., et al. 2003. Regulation and function of the interleukin 13 receptor alpha 2 during a T helper cell type 2-dominant immune response. *J. Exp. Med.* **197**:687–701.
19. Rahaman, S.O., et al. 2002. IL-13R (alpha)2, a decoy receptor for IL-13 acts as an inhibitor of IL-4-dependent signal transduction in glioblastoma cells. *Cancer Res.* **62**:1103–1109.
20. Tabata, Y., et al. 2006. Allergy-driven alternative splicing of IL-13 receptor {alpha}2 yields distinct membrane and soluble forms. *J. Immunol.* **177**:7905–7912.
21. Kellner, J., et al. 2006. IL-13Ralpha2 reverses the effects of IL-13 and IL-4 on bronchial reactivity and acetylcholine-induced Ca signaling. *Int. Arch. Allergy Immunol.* **142**:199–210.
22. Taga, K., Mostowski, H., and Tosato, G. 1993. Human interleukin-10 can directly inhibit T-cell growth. *Blood.* **81**:2964–2971.
23. Moore, K.W., de Waal Malefyt, R., Coffman, R.L., and O'Garra, A. 2001. Interleukin-10 and the interleukin-10 receptor. *Annu. Rev. Immunol.* **19**:683–765.
24. Perona-Wright, G., et al. 2006. Distinct sources and targets of IL-10 during dendritic cell-driven Th1 and Th2 responses in vivo. *Eur. J. Immunol.* **36**:2367–2375.
25. Balic, A., Harcus, Y.M., Taylor, M.D., Brombacher, F., and Maizels, R.M. 2006. IL-4R signaling is required to induce IL-10 for the establishment of Th2 dominance. *Int. Immunol.* **18**:1421–1431.
26. McKee, A.S., and Pearce, E.J. 2004. CD25+CD4+ cells contribute to Th2 polarization during helminth infection by suppressing Th1 response development. *J. Immunol.* **173**:1224–1231.
27. Hesse, M., et al. 2004. The pathogenesis of schistosomiasis is controlled by cooperating IL-10-producing innate effector and regulatory T cells. *J. Immunol.* **172**:3157–3166.
28. Laouini, D., et al. 2003. IL-10 is critical for Th2 responses in a murine model of allergic dermatitis. *J. Clin. Invest.* **112**:1058–1066. doi:10.1172/JCI200318246.
29. Barbarin, V., Xing, Z., Delos, M., Lison, D., and Huaux, F. 2005. Pulmonary overexpression of IL-10 augments lung fibrosis and Th2 responses induced by silica particles. *Am. J. Physiol. Lung Cell. Mol. Physiol.* **288**:L841–L848.
30. Nakagome, K., et al. 2006. In vivo IL-10 gene delivery attenuates bleomycin induced pulmonary fibrosis by inhibiting the production and activation of TGF-β in the lung. *Thorax.* **61**:886–894.
31. Nakagome, K., et al. 2005. In vivo IL-10 gene delivery suppresses airway eosinophilia and hyperreactivity by down-regulating APC functions and migration without impairing the antigen-specific systemic immune response in a mouse model of allergic airway inflammation. *J. Immunol.* **174**:6955–6966.
32. Helmby, H., and Grencis, R.K. 2003. Contrasting roles for IL-10 in protective immunity to different life cycle stages of intestinal nematode parasites. *Eur. J. Immunol.* **33**:2382–2390.
33. van Scott, M.R., et al. 2000. IL-10 reduces Th2 cytokine production and eosinophilia but augments airway reactivity in allergic mice. *Am. J. Physiol. Lung Cell. Mol. Physiol.* **278**:L667–L674.
34. Tournoy, K.G., Kips, J.C., and Pauwels, R.A. 2000. Endogenous interleukin-10 suppresses allergen-induced airway inflammation and nonspecific airway responsiveness. *Clin. Exp. Allergy.* **30**:775–783.
35. Hadeiba, H., and Locksley, R.M. 2003. Lung CD25 CD4 regulatory T cells suppress type 2 immune responses but not bronchial hyperreactivity. *J. Immunol.* **170**:5502–5510.
36. Kearley, J., Barker, J.E., Robinson, D.S., and Lloyd, C.M. 2005. Resolution of airway inflammation and hyperreactivity after in vivo transfer of CD4+CD25+ regulatory T cells is interleukin 10 dependent. *J. Exp. Med.* **202**:1539–1547.
37. Justice, J.P., et al. 2001. IL-10 gene knockout attenuates allergen-induced airway hyperresponsiveness in C57BL/6 mice. *Am. J. Physiol. Lung Cell. Mol. Physiol.* **280**:L363–L368.
38. Makela, M.J., et al. 2000. IL-10 is necessary for the expression of airway hyperresponsiveness but not pulmonary inflammation after allergic sensitization. *Proc. Natl. Acad. Sci. U. S. A.* **97**:6007–6012.
39. Grunig, G., et al. 1997. Interleukin-10 is a natural suppressor of cytokine production and inflammation in a murine model of allergic bronchopulmonary aspergillosis. *J. Exp. Med.* **185**:1089–1099.
40. Kamanaka, M., et al. 2006. Strong expression of interleukin-10 in intestinal lymphocytes after TCR stimulation in vivo detected by an interleukin-10 knockin tiger mouse. *Immunity.* **25**:941–952.
41. Lack, G., et al. 1996. Nebulized IFN-gamma inhibits the development of secondary allergic responses in mice. *J. Immunol.* **157**:1432–1439.
42. Schwarze, J., et al. 1998. Local treatment with IL-12 is an effective inhibitor of airway hyperresponsiveness and lung eosinophilia after airway challenge in sensitized mice. *J. Allergy Clin. Immunol.* **102**:86–93.
43. Pouladi, M.A., et al. 2004. Interleukin-13-dependent expression of matrix metalloproteinase-12 is required for the development of airway eosinophilia in mice. *Am. J. Respir. Cell Mol. Biol.* **30**:84–90.
44. McMillan, S.J., et al. 2004. Matrix metalloproteinase-9 deficiency results in enhanced allergen-induced airway inflammation. *J. Immunol.* **172**:2586–2594.
45. Lee, C.G., et al. 2002. Transgenic overexpression of interleukin (IL)-10 in the lung causes mucus metaplasia, tissue inflammation, and airway remodeling via IL-13-dependent and -independent pathways. *J. Biol. Chem.* **277**:35466–35474.
46. Nakanishi, A., et al. 2001. Role of gob-5 in mucus overproduction and airway hyperresponsiveness in asthma. *Proc. Natl. Acad. Sci. U. S. A.* **98**:5175–5180.
47. Jakubzick, C., et al. 2004. Human pulmonary fibroblasts exhibit altered interleukin-4 and interleukin-13 receptor subunit expression in idiopathic interstitial pneumonia. *Am. J. Pathol.* **164**:1989–2001.
48. Feng, N., et al. 1998. The interleukin-4/interleukin-13 receptor of human synovial fibroblasts: overexpression of the nonsignaling interleukin-13 receptor alpha2. *Lab. Invest.* **78**:591–602.
49. Zheng, T., et al. 2003. Cytokine regulation of IL-13Ralpha2 and IL-13Ralpha1 in vivo and in vitro. *J. Allergy Clin. Immunol.* **111**:720–728.
50. Tang, L., et al. 2001. Recombinant canine IL-13 receptor alpha2-Fc fusion protein inhibits canine allergen-specific-IgE production in vitro by peripheral blood mononuclear cells from allergic dogs. *Vet. Immunol. Immunopathol.* **83**:115–122.
51. Morse, B., Sypek, J.P., Donaldson, D.D., Haley, K.J., and Lilly, C.M. 2002. Effects of IL-13 on airway responses in the guinea pig. *Am. J. Physiol. Lung Cell. Mol. Physiol.* **282**:L44–L49.
52. Taube, C., et al. 2002. The role of IL-13 in established allergic airway disease. *J. Immunol.* **169**:6482–6489.
53. Miyahara, S., et al. 2006. IL-13 is essential to the late-phase response in allergic rhinitis. *J. Allergy Clin. Immunol.* **118**:1110–1116.
54. Grunig, G., et al. 2002. Roles of interleukin-13 and interferon-gamma in lung inflammation. *Chest.* **121**(3 Suppl.):88S.
55. Kumar, R.K., Webb, D.C., Herbert, C., and Foster, P.S. 2006. Interferon-gamma as a possible target in chronic asthma. *Inflamm. Allergy Drug Targets.* **5**:253–256.
56. Mentink-Kane, M.M., et al. 2004. IL-13 receptor alpha 2 down-modulates granulomatous inflammation and prolongs host survival in schistosomiasis. *Proc. Natl. Acad. Sci. U. S. A.* **101**:586–590.
57. Jakubzick, C., et al. 2002. Interleukin-13 fusion cytotoxin arrests Schistosoma mansoni egg-induced pulmonary granuloma formation in mice. *Am. J. Pathol.* **161**:1283–1297.
58. Cheever, A.W., et al. 1994. Anti-IL-4 treatment of Schistosoma mansoni-infected mice inhibits development of T cells and non-B, non-T cells expressing Th2 cytokines while decreasing egg-induced hepatic fibrosis. *J. Immunol.* **153**:753–759.
59. Hamelmann, E., et al. 1997. Noninvasive measurement of airway responsiveness in allergic mice using barometric plethysmography. *Am. J. Respir. Crit. Care Med.* **156**:766–775.
60. Komlosi, Z.I., et al. 2006. Lipopolysaccharide exposure makes allergic airway inflammation and hyper-responsiveness less responsive to dexamethasone and inhibition of iNOS. *Clin. Exp. Allergy.* **36**:951–959.
61. Finkelman, F.D., and Morris, S.C. 1999. Development of an assay to measure in vivo cytokine production in the mouse. *Int. Immunol.* **11**:1811–1818.
62. Pesce, J., et al. 2006. The IL-21 receptor augments Th2 effector function and alternative macrophage activation. *J. Clin. Invest.* **116**:2044–2055. doi:10.1172/JCI27727.